Coherent population trapping with high common-mode noise rejection using differential detection of simultaneous dark and bright resonances

Peter Yun[1],* Rodolphe Boudot[2], and Emeric de Clercq[3]
[1] *National Time Service Center, Chinese Academy of Sciences, 710600 Xi'an, People's Republic of China.*
[2] *FEMTO-ST, CNRS, Université Bourgogne Franche-Comté, Besançon, France. and*
[3] *SYRTE, Observatoire de Paris, Paris, France.*
(Dated: December 13, 2022)

Coherent manipulation of atomic states is highly desired in numerous applications spanning from fundamental physics to metrology. In this study, we propose and demonstrate, theoretically and experimentally, the simultaneous observation in a vapor cell of dark and bright resonances that provide, through a differential detection stage, an output coherent population trapping atomic resonance that benefits from a doubled amplitude and high common-mode noise rejection. This advanced spectroscopic scheme might be of interest for the development of high-performance vapor cell atomic clocks, sensors, or high-resolution spectroscopy experiments.

I. INTRODUCTION

Driving two atomic transitions that share a common excited level with a coherent bi-chromatic light field in a Λ-scheme yields, through electromagnetically induced transparency (EIT) [1], the detection of a narrow atomic resonance line at the output of the atomic medium. This spectroscopic feature, explained by coherent population trapping (CPT) [2–4] of atoms into a quantum dark state [5], can exhibit a linewidth several orders of magnitude lower than the natural linewidth of the optical transitions. CPT has since been implemented in a plethora of applications, including the demonstration of compact [6–9] and miniaturized cell-based atomic clocks [10], optical frequency references [11–13], magnetometers [14], atom laser cooling [15, 16], quantum information science [17], or slow-light experiments [18].

The counterpart effect to EIT is electromagnetically induced absorption (EIA). This phenomenon, discovered in [19] and initially explained in [20], can be also observed in 3-level Λ-systems by using two counter-propagating bichromatic light fields with properly chosen polarizations and mutual phase delay, such that a dark state created by one dual-frequency light field is a bright state for the other [21]. The detection of two-photon EIA resonances was recently applied for the demonstration of a vapor cell atomic clock [22] or combined with pulsed interrogation for the observation of sub-kHz Ramsey-narrowed EIA resonances [23].

CPT and EIA-based vapor cell atomic clocks have demonstrated short-term fractional frequency stability levels, at 1 s integration time, in the low 10^{-13} range [6, 8, 9] and 4×10^{-12}, respectively [22]. Although remarkable, these performances remain about one order of magnitude worse than the ultimate photon shot noise limit [24], i.e., at the level of a few $10^{-14}\ \tau^{-1/2}$ (with τ the integration time). Thus, it is of crucial importance to propose innovative CPT pumping schemes that might tackle this remaining obstacle. In CPT spectroscopy, numerous optimized double-Λ schemes have been proposed to increase the CPT signal [25–29, 31–34]. In addition, several differential detection schemes have been proposed to mitigate the laser noise that usually pollutes the resonance signal [35–37].

In this work, we propose and demonstrate a method for the detection of coherent superposition state resonances with enhanced signal-to-noise ratio through the simultaneous detection of EIT and EIA resonances and a subsequent differential detection stage. Initially prepared into a CPT state that can employ various interaction schemes [25–27, 31, 33], atoms are then interrogated with a finely phase-delayed linearly polarized bichromatic probe beam, such that the initial CPT state is a dark state or bright state for respective orthogonal circularly-polarized components of the probe field. Explained by the fact that one of the four electric dipole moments involved in the double-Λ system of the alkali-atom D_1 line is of opposite sign to the other three, EIT and EIA resonances are then simultaneously generated. These two orthogonally-polarized signals are then optically separated at the cell output and subtracted from each other, yielding an output signal with enhanced amplitude and suppressed common noise. Experimental results are well-explained by a dedicated model and are promising towards the demonstration of a high-performance vapor cell CPT clock.

II. BASIC THEORY

The principle of our approach is depicted in Figure 1. The interaction Hamiltonian of the simplified four-level atomic scheme is [33]

$$\begin{aligned} V_1 =& V_{1+} + V_{1-} \\ =& \frac{-\hbar}{2}(\Omega_1^{'}|3\rangle\langle 1| + \Omega_2^{'}|3\rangle\langle 2| + H.C.) + \\ & \frac{-\hbar}{2}(\Omega_3^{'}|4\rangle\langle 1| + \Omega_4^{'}|4\rangle\langle 2| + H.C.), \end{aligned} \tag{1}$$

* Corresponding author: yunenxue@ntsc.ac.cn, permanent e-mail: yunenxue@163.com

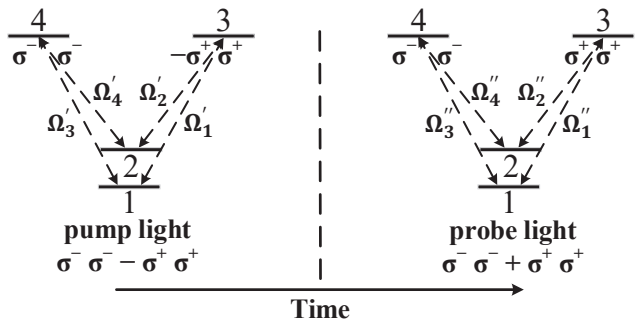

FIG. 1. Principle of the double-Λ four-level system, coupled successively with the pump and probe light. Note the sign difference of one σ^+ polarization component between the pump and probe light.

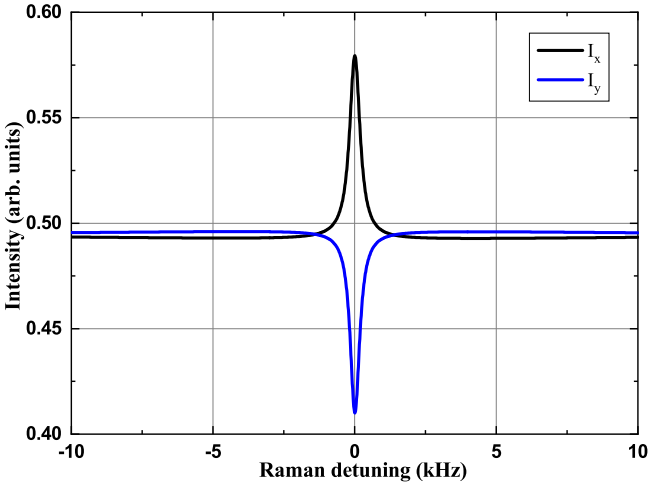

FIG. 2. Transmitted light signals obtained with theoretical calculation. I_x, I_y are the intensities on both orthogonal polarization axis. Parameter values are Rabi frequency $\Omega/(2\pi) = 0.06\,\mathrm{MHz}$, excited state to ground state decay rate $\Gamma/(2\pi) = 0.6\,\mathrm{GHz}$, ground-state coherence decay rate $\gamma_2/(2\pi) = 200\,\mathrm{Hz}$, electric field ratio of probe to pump beam $k_0 = 1/\sqrt{2}$, $\tau_1 = 4.5\,\mathrm{ms}$, $t_d = 4.502\,\mathrm{ms}$, $t_w = 30\,\mu\mathrm{s}$. Parameters of the time sequence are defined in Fig.3.

where H.C. stands for the Hermitian conjugate, and $\Omega_{3(4)}^{'} = \Omega e^{i\phi_{3(4)}^{'}}$, $\Omega_1^{'} = \Omega e^{i\phi_1^{'}}$, $\Omega_2^{'} = -\Omega e^{i\phi_2^{'}}$. We note that $\Omega = d\mathcal{E}_0/\hbar$ is the Rabi frequency, with d the electric dipole matrix element of the transition, and $\mathcal{E}_0$ the amplitude of the laser electric field. The minus sign of the last term is due to the opposite sign of its electric dipole moment, compared to the other three, such that $-d_{23} = d_{24} = d_{13} = d_{14} = d$, and $\phi_i^{'}$ (i=1,...,4) is the phases of each frequency component.

In the rotating frame and at resonance, the dark and bright states prepared by one circularly polarized (let's say σ^+) bichromatic light can be written respectively as

$$\begin{cases} |d_{1+}\rangle = \cos\ \theta_+ |1\rangle - \sin\ \ \theta_+ |2\rangle, \\ |b_{1+}\rangle = \sin^*\theta_+ |1\rangle + \cos^*\theta_+ |2\rangle, \end{cases} \tag{2}$$

where $\sin\theta_+ = \Omega_1^{'}/\sqrt{|\Omega_1^{'}|^2 + |\Omega_2^{'}|^2}$, $\cos\theta_+ = \Omega_2^{'}/\sqrt{|\Omega_1^{'}|^2 + |\Omega_2^{'}|^2}$. Similarly, we can write the dark $|d_{1-}\rangle$ and bright $|b_{1-}\rangle$ states for the counter-rotated circularly polarized (σ^-) bichromatic light. Each dark state is decoupled from its pump light, i.e.: $\langle 3| V_{1+} |d_{1+}\rangle = 0$, $\langle 4| V_{1-} |d_{1-}\rangle = 0$.

In our study, atoms were prepared in a CPT state using a double-Λ system obtained with the push-pull optical pumping (PPOP) scheme [25, 26]. In this scheme, a Michelson system is employed to introduce a phase delay and compensate the opposite sign of d_{23}, i.e., $\phi_+^{'} = \phi_-^{'} + (2p_1 + 1)\pi$, with $\phi_{+(-)}^{'} = \phi_{1(3)}^{'} - \phi_{2(4)}^{'}$, and p_i $(i = 1 - 4)$ an arbitrary integer. The atom-light interaction for pumping the atoms in the CPT state is then denoted $\sigma^-\sigma^- - \sigma^+\sigma^+$, as shown in Fig. 1. In this configuration, we arrive, with an appropriate phase, to $|d_{1+}\rangle = |d_{1-}\rangle \equiv |d_1\rangle$, meaning that each dark state built by one circular polarization is also a dark state for the counter-rotating polarization.

In the second step shown in Fig. 1, the atomic ensemble is probed by a linearly polarized bichromatic beam. Since the σ^+ and σ^- polarization components of this field are in-phase in this case, i.e. $\phi_+^{''} = \phi_-^{''} + 2p_2\pi$, with $\phi_{+(-)}^{''} = \phi_{1(3)}^{''} - \phi_{2(4)}^{''}$, the dark states previously-created $|d_1\rangle$ will be coupled or uncoupled to the probe light, depending on whether the interaction field is σ^+ or σ^- polarized. The interaction of the atomic ensemble with the probe field is denoted $\sigma^-\sigma^- + \sigma^+\sigma^+$, as shown in Fig. 1.

The interaction Hamiltonian for the σ^+ component of the probe beam is

$$V_{2+} = \frac{-\hbar}{2}(\Omega_1^{''} |3\rangle\langle 1| + \Omega_2^{''} |3\rangle\langle 2| + H.C.). \tag{3}$$

A proper phase delay setting between probe and pump light, e.g. $\phi_+^{'} - \phi_+^{''} = 2p_3\pi$, leads to $V_{2+} |d_1\rangle = 0$. In this case, the previous dark state remains a dark state and EIT is observed. At the opposite, for the σ^- component, the reverse applies since $\phi_-^{'} - \phi_-^{''} = (2p_4 + 1)\pi$, leading to $V_{2-} |d_1\rangle \neq 0$. In this case, the previous dark state becomes a bright state and EIA occurs.

Based on this 4-level model, we have also performed numerical calculations using the Liouville equation (see Appendix). Figure 2 shows the calculated signals at both outputs of a polarizing beam splitter (PBS) placed at the cell output. It clearly demonstrates the simultaneous presence of EIT and EIA resonances detected at null Raman detuning. Once obtained, a differential CPT signal can be obtained by subtracting EIT and EIA signals. We note here that our scheme, in comparison with previously-reported differential detection schemes [35–37], offers an ideal differential detection with doubled amplitude of the signal and rejection of the common-mode noise.

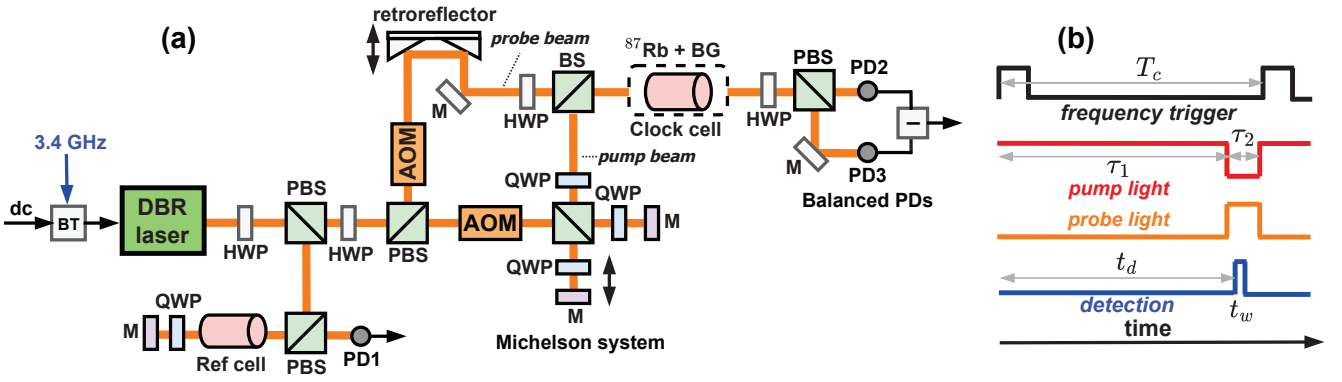

FIG. 3. (a): Experimental setup. BS: non-polarizing beamsplitter, PBS: polarizing beamsplitter, PD: photodetector, AOM: acousto-optic modulator, QWP: quarter-wave plate, HWP: half-wave plate, M: mirror, BT: bias-tee. (b): Time sequence for CPT spectroscopy.

III. EXPERIMENTAL SET-UP

Using this concept, the experimental setup depicted in Fig. 3, based on the one described in [9], was implemented. A distributed Bragg reflector (DBR) laser is directly modulated at 3.417 GHz in order to produce a multi-frequency laser field, such that both first-order optical sidebands are used for CPT interaction. The light beam is then separated into three arms. The first arm is used to stabilize the laser carrier frequency to the midpoint of the two transitions of the ^{87}Rb D_1 line i.e., $|5^2S_{1/2}, F = 1\&2\rangle \rightarrow |5^2P_{1/2}, F^{'} = 2\rangle$, using dual-frequency sub-Doppler spectroscopy [11] in a vacuum reference cell. The second arm is directed to a Michelson system in order to produce two phase-delayed counter-rotating circularly polarized dual-frequency light fields and then to generate the PPOP scheme used as the pumping field. The third arm is used to prepare the probing light field. The latter is properly phase delayed relative to one arm of the Michelson interferometer, while a half-wave plate is used to tune its polarization plane. The pump and probe beams are overlapped with the help of a non-polarizing beamsplitter (BS). Two acousto-optic modulators (AOM), both driven at 180 MHz, are used to switch on and off the pump and probe lights. These AOMs also compensate for the buffer-gas-induced optical frequency shift in the clock cell. The pump and probe beams are expanded to a circular beam with $1/e^2$ diameter of about 5 mm before the clock cell. The ^{87}Rb isotope enriched cylindrical vapor cell (diameter: 20 mm, length: 50 mm) is filled with a N_2-Ar buffer gas mixture, and temperature stabilized around 54.6 °C. Unless otherwise specified, a uniform axial static magnetic field $B_0 = 14.6\,\mu$T is applied to raise the Zeeman degeneracy. The ensemble is surrounded by one layer of mu-metal magnetic shield. At the cell output, the transmitted light is polarization rotated by $\pi/4$ with respect to the axis of the following polarizing beam splitter (PBS), then separated in two paths by the PBS, and finally detected by balanced photodetectors (PD).

The pump and probe light beams interact with the atomic ensemble using the sequence shown in Fig. 3(b), with T_c the cycle time. Atoms are first prepared in CPT states during a pumping stage of length τ_1, usually of several milliseconds. At the end of this pumping stage, a probing-light window, of length τ_2, much smaller than τ_1, is opened. The PD signals are then recorded during a short detection window of length t_w, in the range of 30 µs − 100 µs, which follows, after a delay time of 2 µs, the probe light activation. In our system, the detection window time is tuned such that $0 < t_w \leq \tau_{deph} \leq \tau_2$, with $\tau_{deph} \approx 1$ ms in our experiment, is the time for the two previously-prepared dark states to become common bright states and interact each other. Ramsey-CPT interrogation can be also performed by inserting a free-evolution dark time, of length T, between the end of the pumping window and the start of the probing window.

IV. EXPERIMENTAL RESULTS

Figure 4 shows typical simultaneously-observed EIT, EIA and differential-CPT (diff-CPT) experimental signals. Narrow linewidth and high-contrast (14.4%) EIT and EIA signals are obtained. The three peaks correspond to respective $\Delta m_F = 0$ transitions between sub-levels of magnetic quantum number $m_F = -1, 0, +1$, respectively, with the central peak being the clock transition. The amplitude asymmetry of lateral peaks ($m_F = \pm 1$) between EIT and EIA signals can be explained by a residual elliptic polarization and optical pumping effects. Indeed, the σ^- component of the probe beam, for which the previously created dark states are now bright states, pumps atoms toward lower magnetic number Zeeman sub-levels, whereas the σ^+ component, for which the previously created dark states remain dark, pumps atoms toward higher magnetic number Zeeman sub-levels. Compared to EIT and EIA signals, the diff-

CPT signal is detected with a dc background level that is almost nulled and its amplitude is two times higher. This configuration is then favorable for achieving a CPT resonance with high contrast (usually defined as the ratio between the resonance amplitude and its dc background level). The linewidth of the diff-CPT signal is between those of EIT and EIA resonances. More important, the common-mode noise is highly rejected, as better highlighted in the following section.

We have measured the dependence of the resonance amplitude, linewidth (FWHM), and the SNR/linewidth ratio on the laser pump power, for EIT, EIA and diff-CPT signals. Here, the SNR is defined as $SNR = A_{CPT}/N$, where A_{CPT} is the CPT amplitude (CPT maximum minus the Doppler-broadened absorption background), while the noise N is the typical fluctuation at 1 s of the signal measured at half maximum of the detected CPT resonance [38]. Results are shown in Fig. 5. The linewidth increases with the pump power, while the amplitude saturates for powers higher than about 350 μW. The SNR/linewidth is maximized for laser powers lower than 50 μW. This ratio is more than three times higher in the case of the diff-CPT signal, in the region of interest. We have performed a comparable test as a function of the laser probe power. In this case, we found that the linewidth remains about constant while the amplitude increases for all cases. The SNR/FWHM was maximized at a probe power of 48 μW.

An important feature of the proposed spectroscopic

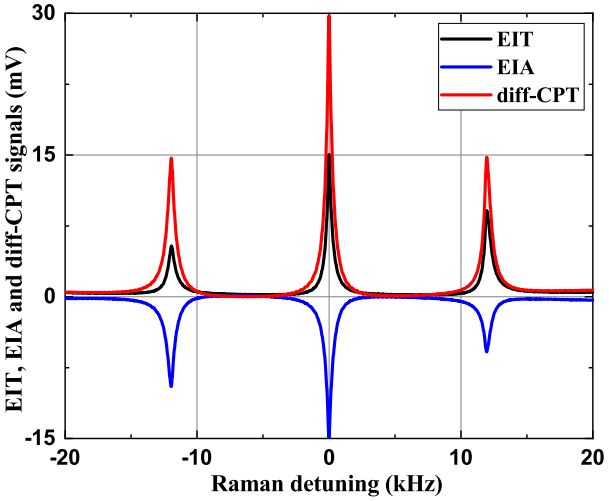

FIG. 4. Experimentally-observed EIT, EIA and diff-CPT signals. Experimental parameters are: $T_c = 3.1$ ms, $\tau_1 = 3$ ms, $\tau_2 = 0.1$ ms, $t_d = 3.002$ ms, $t_w = 0.03$ ms, $B_0 = 0.87$ µT, $P_{pump} = 107$ µW, $P_{probe} = 57$ µW. An offset of 103.2 and 103.4 mV was subtracted to EIT and EIA signals, respectively. The diff-CPT signal is detected with a dc background level that is almost nulled, and exhibits amplitude two times higher than those of EIA and EIT resonances. This figure shows the photodiodes' outputs in working conditions, with both PD2 and PD3 illuminated by incident light.

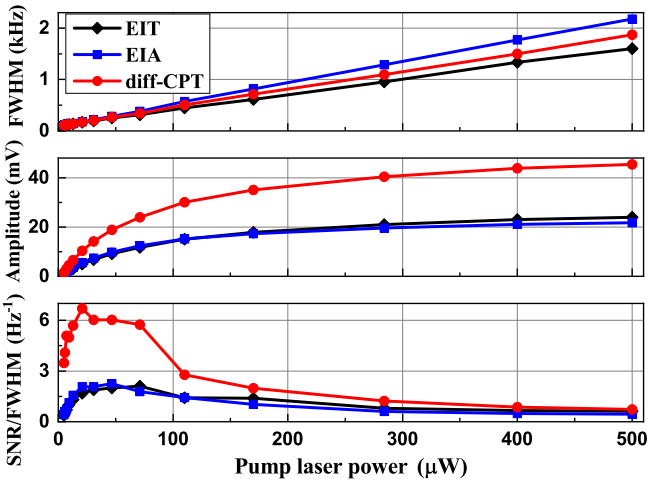

FIG. 5. Signal linewidth, amplitude and SNR/FWHM ratio of EIT, EIA and diff-CPT amplitude as a function of the laser pump power. Experimental parameters are: $T_c = 4.6$ ms, $\tau_1 = 4.5$ ms, $\tau_2 = 0.1$ ms, $t_d = 4.502$ ms, $t_w = 0.03$ ms, $P_{probe} = 57$ µW. Solid lines are here to guide the eye of the reader.

approach is the expected rejection of the common-mode noise on the differential CPT signal. This property is clearly demonstrated in Fig. 6, in the case of a measurement at low laser power (here, 6 μW). In this configuration, the SNR of the diff-CPT signal is improved by a factor of almost 10, in comparison with those obtained for initial EIT and EIA signals. We observe that the noise mitigation obtained with the proposed method is here better, at low power, than the one obtained at a higher power (see Fig. 5(c)). This dependence on the laser power of the noise mitigation factor is not clear to date and will be investigated in a dedicated future study. We note eventually that the diff-CPT resonance exhibits on Fig. 6 a narrow linewidth of 97 Hz.

For further investigation, we have also measured the noise spectrum of the error signal when a local oscillator (LO) is locked to the atomic resonance [39]. In this evaluation, we use a standard synchronous modulation-demodulation technique of the microwave frequency, with FM depth of about 85 Hz and FM period $T_{FM} = 2\ T_c$, to generate an error signal which might be used to stabilize the LO frequency. The noise spectrum of the error signal is then measured in closed loop operation of the atomic clock with a noise analyzer (Stanford Research Systems, SR785). Noise spectra obtained for EIT, EIA and diff-CPT error signals, as well as error signals themselves, are shown on Fig. 7.

On noise spectra shown in Fig. 7, the noise valleys at 13.6 Hz and its harmonics are suspected to come from the feedback rate $1/T_{FB}$, with one feedback applied every 8 FM cycle periods, i.e., $T_{FB} = 8\ T_{FM}$. Most importantly, the noise level of the diff-CPT error signal is highly reduced. This result suggests that our method should help to improve the performances of CPT clocks, includ-

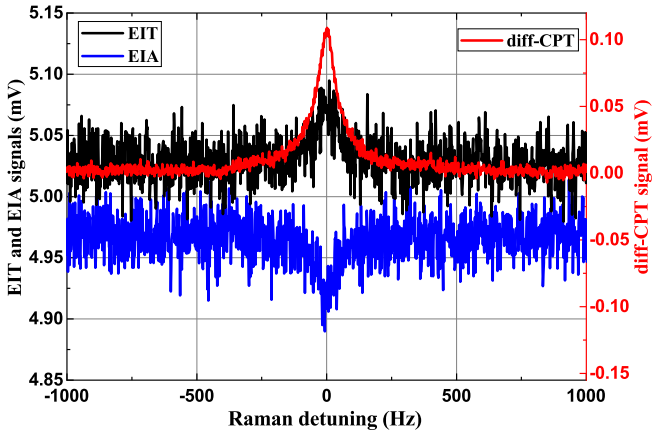

FIG. 6. EIT, EIA and diff-CPT signals obtained for a low laser power record. Experimental parameters are: $T_c = 4.6\,\text{ms}$, $\tau_1 = 4.5\,\text{ms}$, $\tau_2 = 0.1\,\text{ms}$, $t_d = 4.502\,\text{ms}$, $t_w = 0.03\,\text{ms}$, $P_{pump} = 6.1\,\mu\text{W}$, $P_{probe} = 5.9\,\mu\text{W}$. For this plot, the EIA is down shifted for clarity. The SNR of the diff-CPT signal is about 10 times higher than EIT and EIA signals.

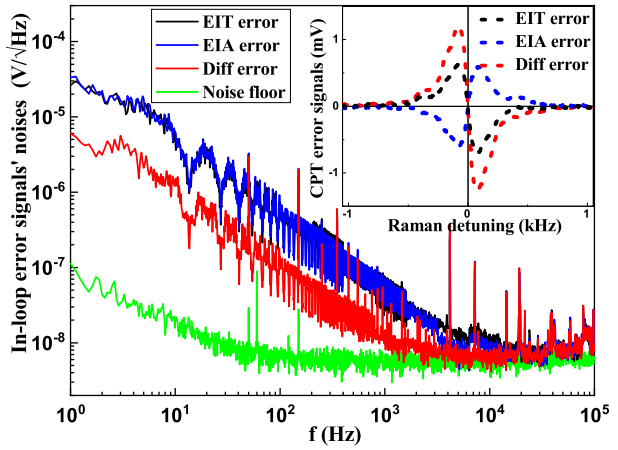

FIG. 7. Noise of in-loop error signals, for EIT, EIA and diff-CPT cases. Experimental parameters are: $T_c = 4.61\,\text{ms}$, $\tau_1 = 4.5\,\text{ms}$, $\tau_2 = 0.11\,\text{ms}$, $t_d = 4.502\,\text{ms}$, $t_w = 0.1\,\text{ms}$, $P_{pump} = 30.7\,\mu\text{W}$, $P_{probe} = 11.8\,\mu\text{W}$. The noise floor of the analyzer is also plotted for information. The inset shows the EIT, EIA and diff-CPT error signals with the same conditions.

ing those based on push-pull optical pumping [40, 41], dominated by laser AM-AM and FM-AM noise sources. Specifically, the noise amplitude of the diff-CPT signal was here divided by 4.5 compared to EIT and EIA cases in the $1\,\text{Hz} - 1\,\text{kHz}$ offset range. Thus, the frequency stability of the atomic clock using the diff-CPT signal should be about 4.5 times better than one based on EIT or EIA signals.

We have also observed the spectral lineshape of $|F = 1, m_F = \pm 1\rangle \leftrightarrow |F = 2, m_F = \mp 1\rangle$ transitions in the present configuration. These $\Delta m_F = \pm 2$ transitions, shown on Fig. 8, are well separated from the clock transition at "high" magnetic field (here $B_0 = 233\,\mu\text{T}$). Their shape is different from those observed in [26, 30]. For $\Delta m_F = -2$, an EIT signal is observed for the clock transition EIT channel, while an EIA signal is obtained in the clock transition EIA channel. In the case of $\Delta m_F = +2$, the reverse applies. Again, the differential signal, i.e. EIT channel minus EIA channel, shows here a higher SNR. This observation shows that our method can be also applied to the lin‖lin CPT scheme [28]. To apply this idea, both pump and probe beams should be linearly polarized, with the probe beam polarization axis rotated by 45° relative to the pump light polarization. If one of the two polarization components of the probe beam, let's say on the x-axis, induces EIT, the orthogonal component will induce EIA. With a similar polarization separation, we can then simultaneously observe EIT, EIA and differential CPT signals in the lin‖lin scheme.

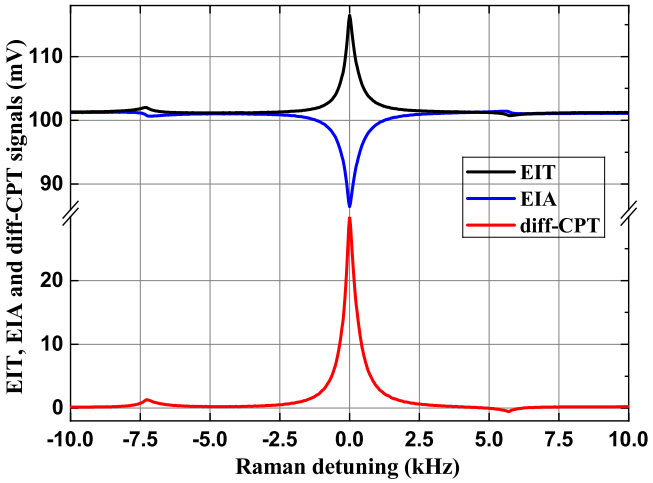

FIG. 8. EIT, EIA and diff-CPT signals with $\Delta m_F = 0$ and $\Delta m_F = \pm 2$. Experimental parameters are: $T_c = 4.6\,\text{ms}$, $\tau_1 = 4.5\,\text{ms}$, $\tau_2 = 0.1\,\text{ms}$, $t_d = 4.502\,\text{ms}$, $t_w = 0.03\,\text{ms}$, $P_{pump} = 107\,\mu\text{W}$, $P_{probe} = 57\,\mu\text{W}$. The static magnetic field is $B_0 = 233\,\mu\text{T}$. The clock transition is here shifted by 3.128 kHz, in comparison with previous cases, due to the second-order Zeeman shift.

In a last part, we succeeded to detect experimental Ramsey fringes of EIT, EIA and diff-CPT by applying a pulsed interrogation sequence. Similarly to other Ramsey-CPT clocks [27, 41], this regime was obtained by inserting a free-evolution dark time, of length T, between the end of the pumping window and the start of the probing window. Obtained Ramsey fringes of EIT, EIA and diff-CPT, with $T = 5\,\text{ms}$, are shown in Fig. 9.

A narrow fringe linewidth of 78.2 Hz is observed for $T = 5\,\text{ms}$. Here again, we note that the amplitude of the central fringe is doubled in the case of the diff-CPT signal. For infomation, we have measured the CPT coherence relaxation time T_2 for each channel, by varying the Ramsey time T. We found respectively for EIT, EIA, and diff-CPT signals T_2 coherence times of 4.40(4) ms, 5.33(25) ms, and 4.88(11) ms.

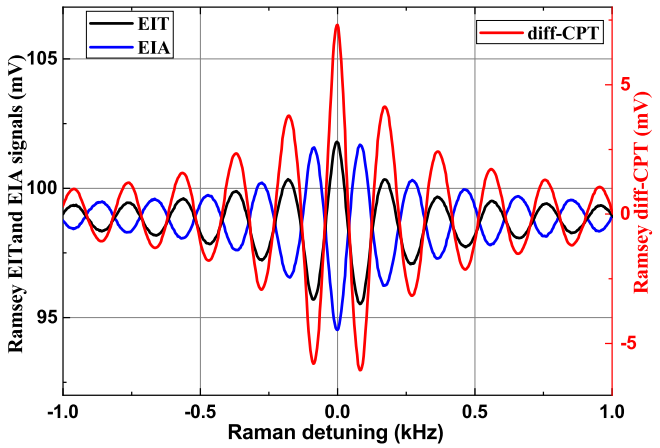

FIG. 9. Ramsey EIT, EIA and diff-CPT signals. Experimental parameters are: $T_c = 9.6\,\text{ms}$, $\tau_1 = 4.5\,\text{ms}$, $T = 5\,\text{ms}$, $\tau_2 = 0.1\,\text{ms}$, $t_d = 9.502\,\text{ms}$, $t_w = 0.03\,\text{ms}$, $P_{pump} = 107\,\mu\text{W}$, $P_{probe} = 57\,\mu\text{W}$.

V. CONCLUSIONS

In conclusion, we have proposed and demonstrated, theoretically and experimentally, a spectroscopic approach for simultaneous observation in a single atomic ensemble of EIT and EIA signals. Subsequent extraction of a differential signal at the cell output allows the detection of a CPT resonance with a doubled amplitude and high common-mode noise rejection. This method relies on the use of double-Λ schemes for which one of the four involved dipolar moments is of opposite sign to others. This method is then quite universal since the pumping light can use various optimized CPT pumping schemes [25–29, 31–33], including the lin$\|$lin scheme [28], and can be also applied to other alkali metal atoms. The proposed approach might be of great interest for the development of a high-performance CPT clock, possibly surpassing state-of-the-art stability results of current CPT clocks [6, 8, 9] and approaching the long-sought level of a few $10^{-14}\tau^{-1/2}$ predicted by the photon shot noise limit [24].

ACKNOWLEDGEMENTS

We gratefully acknowledge Thomas Zanon-Willette (Sorbonne Université), Moustafa Abdel Hafiz (FEMTO-ST) and James McGilligan (University of Strathclyde) for careful reading of the manuscript and constructive suggestions. This work was funded by the National Natural Science Foundation of China (Grant No. 12173043, Grant No. U1731132). R. B was supported by Région Bourgogne Franche-Comté in the frame of the HACES project and by the LabeX FIRST-TF (Grant ANR 10-LABX-0048).

Appendix: THEORETICAL SIMULATION

In this appendix, we show how EIT and EIA signals simultaneously occur. This study is extracted from theoretical simulations based on the 4-level model shown in Fig. 1, using the Liouville equation and the polarization rotation calculation method.

1. The pump and probe light fields

The bichromatic light is described by a classical field with angular frequency $\omega_\pm$ propagating along the z-axis. The electric field of the pump light can be represented by:

$$\boldsymbol{E_{pump}} = \mathcal{E}_0 f_a(t)\{[\cos(\omega_+ t + \phi_1^{'}) + \cos(\omega_- t + \phi_2^{'})]\hat{e}_+ + [\cos(\omega_+ t + \phi_3^{'}) + \cos(\omega_- t + \phi_4^{'})]\hat{e}_-\}. \tag{A.1}$$

During the probe stage, the linearly polarized probe beam, with a polarization angle θ relative to the x-axis, can be written as:

$$\boldsymbol{E_{probe}} = k_0\mathcal{E}_0 f_b(t)[\cos(\omega_+ t + \phi_3^{''}) + \cos(\omega_- t + \phi_4^{''})]\hat{e}_\theta. \tag{A.2}$$

Here k_0 is the amplitude ratio between pump and probe electric fields, $f_a(t) = U[t] - U[t-\tau]$, and $f_b(t) = f_a(t-\tau)$, where U[t] is a step function. In order to take into account the switch times (1 µs) of the pump and probe beams in our experiments, a sine function is used to replace the rising and falling edges of step function.

With the definition: $\hat{e}_\theta = (\cos\theta\hat{e}_+ + \sin\theta\hat{e}_-)/\sqrt{2}$, $\hat{e}_x = -(\hat{e}_+ - \hat{e}_-)/\sqrt{2}$, and $\hat{e}_y = i(\hat{e}_+ + \hat{e}_-)/\sqrt{2}$, we can rewrite:

$$\boldsymbol{E_{probe}} = k_0\mathcal{E}_0 f_b(t) \{[\cos(\omega_+ t + \phi_1^{''}) + \cos(\omega_- t + \phi_2^{''})]e^{-i\theta}\hat{e}_+ + [\cos(\omega_+ t + \phi_3^{''}) + \cos(\omega_- t + \phi_4^{''})]e^{i\theta}\hat{e}_-\}/\sqrt{2}, \tag{A.3}$$

where $\phi_{1(2)}^{''} = \phi_{3(4)}^{''} + m(n)\pi$, m and n are arbitrary odd integer.

2. Polarization rotation of the clock cell transmitted light

Using Jones matrix, and with $\hat{e}_\pm = \mp(\hat{e}_x \pm i\hat{e}_y)/\sqrt{2}$, the electric field (Eq. A.3) of the probe beam can be written as:

$$\boldsymbol{E_{probe}} = \frac{k_0\mathcal{E}_0}{\sqrt{2}}\sum_{\omega_+}^{\omega_-}\left\{e^{-i\theta}\begin{bmatrix}-1\\-i\end{bmatrix}_{\omega_+} + e^{i\theta}\begin{bmatrix}1\\-i\end{bmatrix}_{\omega_+}\right\}. \tag{A.4}$$

From refs [42–44], we know that when the probe beam is transmitted across the clock cell with length L, it is changed to

$$\boldsymbol{E_1} = \frac{k_0\mathcal{E}_0}{\sqrt{2}}\sum_{\omega_+}^{\omega_-}\left\{e^{-i\theta+\xi^+_{\omega_+}}\begin{bmatrix}-1\\-i\end{bmatrix}_{\omega_+} + e^{i\theta+\xi^-_{\omega_+}}\begin{bmatrix}1\\-i\end{bmatrix}_{\omega_+}\right\}, \tag{A.5}$$

with $\xi^{\pm}_{\omega_\pm} = -i\beta^{\pm}_{\omega_\pm} - \alpha^{\pm}_{\omega_\pm}L/2$, $\beta^{\pm}_{\omega_\pm} = 2\pi L n^{\pm}_{\omega_\pm}/\lambda_\pm$, where $n^{\pm}_{\omega_\pm}$ are the refractive indices of the ^{87}Rb atomic medium for the left and right circularly polarized components and $\alpha^{\pm}_{\omega_\pm}$ are the corresponding absorption coefficients.

Thus, by placing at the cell output a half-wave plate characterized by its Jones matrix

$$W_{\lambda/2} = -i\begin{bmatrix}\cos 2\psi & \sin 2\psi\\ \sin 2\psi & -\cos 2\psi\end{bmatrix}, \tag{A.6}$$

we can rotate the polarization of the field $\boldsymbol{E_1}$ with an angle $2\psi = \pi/4 - \theta$. Thus, we obtain the output probe beam with its polarization set to an angle $\pi/4$ relative to the x-axis, for the balance of the two PDs. It reads

$$\boldsymbol{E_2} = W_{\lambda/2}\boldsymbol{E_1} = \frac{-ik_0\mathcal{E}_0}{\sqrt{2}} \sum_{\omega_+}^{\omega_-}\left\{e^{-i\theta+\xi^+_{\omega_+}}\begin{bmatrix}-e^{i2\psi}\\ ie^{i2\psi}\end{bmatrix}_{\omega_+} + e^{i\theta+\xi^-_{\omega_+}}\begin{bmatrix}e^{-i2\psi}\\ ie^{-i2\psi}\end{bmatrix}_{\omega_+}\right\}. \tag{A.7}$$

Thus, for the x-axis polarization detection, with $I_0 = \varepsilon_0(k_0\mathcal{E}_0)^2$, we have:

$$I_x = \frac{I_0}{2}\sum_{\omega_+}^{\omega_-}[e^{-\alpha^+_{\omega_+}L} + e^{-\alpha^-_{\omega_+}L} - 2\sin(4\theta + 2\beta_{\omega_+})e^{-\alpha_{\omega_+}L}]. \tag{A.8}$$

Similarly, for the y-axis polarization detection,

$$I_y = \frac{I_0}{2}\sum_{\omega_+}^{\omega_-}[e^{-\alpha^+_{\omega_+}L} + e^{-\alpha^-_{\omega_+}L} + 2\sin(4\theta + 2\beta_{\omega_+})e^{-\alpha_{\omega_+}L}]. \tag{A.9}$$

In which, $\beta_{\omega_\pm} = (\beta^+_{\omega_\pm} - \beta^-_{\omega_\pm})/2$, $\beta^{\pm}_{\omega_\pm} = 2\pi L n^{\pm}_{\omega_\pm}/\lambda_{\omega_\pm}$, $n^{\pm}_{\omega_\pm} = \sqrt{1 + Re(\chi^{\pm}_{\omega_\pm})}$, $\alpha_{\omega_\pm} = (\alpha^+_{\omega_\pm} + \alpha^-_{\omega_\pm})/2$, $\alpha^{\pm}_{\omega_\pm} = 2\pi Im(\chi^{\pm}_{\omega_\pm})/\lambda_{\omega_\pm}$, and $\chi^{\pm}_{\omega_\pm}$ are the susceptibilities of the atomic medium.

3. Liouville equations

The four-level system shown in Fig. 1 is adopted. The evolution of the density matrix for atoms at rest is given by the Liouville equation,

$$\dot{\rho} = \frac{-i}{\hbar}[H, \rho] - R\rho, \tag{A.10}$$

where $H = H_0 + V$, $H_0 = \hbar\sum_{i=1}^{4}\omega_i\,|i\rangle\,\langle i|$ is the Hamiltonian of the unperturbed atom, ω_i is the angular frequency for level $|i\rangle$. R is the relaxation matrix. The interaction Hamiltonian is $V = -\boldsymbol{D}\cdot(\boldsymbol{E_{pump}} + \boldsymbol{E_{probe}})$, with $\boldsymbol{D}$ the electric dipole operator, it reads

$$\begin{aligned} V = V_+ + V_- =& \frac{-\hbar}{2}(\Omega_1|3\rangle\langle 1| + \Omega_2|3\rangle\langle 2| + H.C.) + \\ & \frac{-\hbar}{2}(\Omega_3|4\rangle\langle 1| + \Omega_4|4\rangle\langle 2| + H.C.), \end{aligned} \tag{A.11}$$

where $\Omega_{1(2)} = \mathcal{E}_0 f_{1(2)}(t)\vec{d}_{1(2)3}\hat{e}_+/\hbar$, $\Omega_{3(4)} = \mathcal{E}_0 f_{3(4)}(t)\vec{d}_{1(2)4}\hat{e}_-/\hbar$, $f_j(t) = f_a(t)e^{-i\phi^{'}_j} + k_0 f_b(t)e^{-i\varphi_j}$, $j = 1-4$, $\varphi_{1(2)} = \phi^{''}_{1(2)} + \theta$, $\varphi_{3(4)} = \phi^{''}_{3(4)} - \theta$.

For simplicity and without loss the generality, we assume that: $\phi^{'}_1 = \phi^{'}_2 = \phi^{'}_3 = 0$, $\phi^{'}_4 = \pi$, and $\phi^{''}_1 = \phi^{''}_2 = \pi$, $\phi^{''}_3 = \phi^{''}_4 = 0$, this lead to: $f_1(t) = f_2(t) = f_a(t) - k_0 f_b(t)e^{-i\theta}$, $f_3(t) = f_a(t) + k_0 f_b(t)e^{i\theta}$, $f_4(t) = -f_a(t) + k_0 f_b(t)e^{i\theta}$, thus we have: $\Omega_1 = -\Omega_2 = \Omega f_1(t)$, $\Omega_3 = \Omega f_3(t)$, $\Omega_4 = \Omega f_4(t)$.

The density matrix evolution is given by

$$\begin{aligned}
\dot{\rho}_{11} &= \Omega Im(\tilde{\rho}_{13}f_1(t)) + \Omega Im(\tilde{\rho}_{14}f_3(t)) + (\rho_{33}+\rho_{44})\Gamma/2 - (\rho_{11}-\rho_{22})\gamma_1,\\
\dot{\rho}_{22} &= -\Omega Im(\tilde{\rho}_{23}f_2(t)) + \Omega Im(\tilde{\rho}_{24}f_4(t)) + (\rho_{33}+\rho_{44})\Gamma/2 - (\rho_{22}-\rho_{11})\gamma_1,\\
\dot{\rho}_{33} &= -\Omega Im(\tilde{\rho}_{13}f_1(t)) + \Omega Im(\tilde{\rho}_{23}f_2(t)) - \rho_{33}\Gamma,\\
\dot{\rho}_{44} &= -\Omega Im(\tilde{\rho}_{14}f_3(t)) - \Omega Im(\tilde{\rho}_{24}f_4(t)) - \rho_{44}\Gamma,\\
\dot{\tilde{\rho}}_{14} &= i[(i\Gamma - 2\pi\Delta)\tilde{\rho}_{14} + (\rho_{44}-\rho_{11})\Omega f^*_3(t) - \tilde{\rho}_{12}\Omega f^*_4(t) + \rho_{34}\Omega f^*_1(t)]/2,\\
\dot{\tilde{\rho}}_{13} &= i[(i\Gamma - 2\pi\Delta)\tilde{\rho}_{13} + (\rho_{33}-\rho_{11})\Omega f^*_1(t) + \tilde{\rho}_{12}\Omega f^*_2(t) + \rho^*_{34}\Omega f^*_3(t)]/2,\\
\dot{\tilde{\rho}}_{24} &= i[(i\Gamma + 2\pi\Delta)\tilde{\rho}_{24} + (\rho_{44}-\rho_{22})\Omega f^*_4(t) - \tilde{\rho}^*_{12}\Omega f^*_3(t) - \rho_{34}\Omega f^*_2(t)]/2,\\
\dot{\tilde{\rho}}_{23} &= i[(i\Gamma + 2\pi\Delta)\tilde{\rho}_{23} - (\rho_{33}-\rho_{22})\Omega f^*_2(t) - \tilde{\rho}^*_{12}\Omega f^*_1(t) + \rho^*_{34}\Omega f^*_4(t)]/2,\\
\dot{\tilde{\rho}}_{12} &= i[(i\gamma_2 - 4\pi\Delta)\tilde{\rho}_{12} + \tilde{\rho}^*_{23}\Omega f^*_1(t) + \tilde{\rho}_{13}\Omega f_2(t) + \tilde{\rho}^*_{24}\Omega f^*_3(t) - \tilde{\rho}_{14}\Omega f_4(t)]/2,\\
\dot{\rho}_{34} &= i[2i\gamma_{43}\rho_{34} - \tilde{\rho}^*_{23}\Omega f^*_4(t) - \tilde{\rho}^*_{13}\Omega f^*_3(t) - \tilde{\rho}_{24}\Omega f_2(t) + \tilde{\rho}_{14}\Omega f_1(t)]/2.
\end{aligned} \tag{A.12}$$

Here we have assumed a solution for the off-diagonal matrix elements of the form: $\rho_{13(4)} = \tilde{\rho}_{13(4)}e^{i\omega_+ t}$, $\rho_{23(4)} = \tilde{\rho}_{23(4)}e^{i\omega_- t}$, $\rho_{12} = \tilde{\rho}_{12}e^{i\omega_{+-} t}$, where $\omega_{+-} = \omega_+ - \omega_-$, and applied the secular approximation. γ_1 and γ_2 are the decay rate of ground-state population and coherence, respectively. Similarly, Γ is the decay rate of population from excited state $|3\rangle$ ($|4\rangle$) to ground state, $\gamma_{31}(\gamma_{32})$, $\gamma_{41}(\gamma_{42})$ are the decay rate of coherence from excited state $|3\rangle$ and $|4\rangle$ to ground state, respectively. γ_{43} is the coherence decay rate between $|4\rangle$ and $|3\rangle$. In typical experiments, we presume $\gamma_1 = \gamma_2$, $\gamma_{31} = \gamma_{32} = \gamma_{41} = \gamma_{42} = \Gamma/2$ and $\gamma_{43} = \Gamma/2000$.

We use these symbols: $\nu_i = \omega_i/(2\pi)$ for $i = 1-4$, $\nu_{+(-)} = \omega_{+(-)}/(2\pi)$, $\nu_{+-} = \omega_{+-}/(2\pi)$, $\nu_{hf} = \nu_2 - \nu_1$, $\nu_{43} = \nu_4 - \nu_3$, $\nu_{31(2)} = \nu_3 - \nu_{1(2)}$, $\nu_{41(2)} = \nu_4 - \nu_{1(2)}$. The two-photon detuning (Raman detuning): $\Delta = \Delta_1 - \Delta_2 = \nu_{+-} - \nu_{hf}$, and the single photo detuning: $\Delta_{1(2)} = \nu_{+(-)} - \nu_{31(2)}$, $\Delta_{3(4)} = \nu_{+(-)} - \nu_{41(2)}$. For simple discussion, we assume $|3\rangle$ and $|4\rangle$ are degenerate ($\nu_{43} = 0$), which means: $\Delta_3 = \Delta_1$, $\Delta_4 = \Delta_2$. In our case where the bichromatic light is obtained by direct modulation of a DBR laser diode at half the ground-state splitting frequency, we have the relation: $\Delta_1 = -\Delta_2 = \Delta/2$.

The initial conditions are:

$$\begin{aligned}
&\rho_{11}(t=0) = \rho_{22}(t=0) = 0.5,\\
&\rho_{33}(t=0) = \rho_{44}(t=0) = 0,\\
&\tilde{\rho}_{12}(t=0) = \tilde{\rho}_{13}(t=0) = \tilde{\rho}_{14}(t=0) =\\
&\tilde{\rho}_{23}(t=0) = \tilde{\rho}_{24}(t=0) = \rho_{34}(t=0) = 0. \quad \text{(A.13)}
\end{aligned}$$

4. Susceptibilities of the atomic medium

For the probe stage, the expressions for the susceptibilities of the atomic medium are $\chi^{\pm}_{\omega_+} = \eta\rho_{3(4)1}$, $\chi^{\pm}_{\omega_-} = \mp\eta\rho_{3(4)2}$, in which $\eta = \dfrac{2N_a d}{\varepsilon_0 E_{probe}}$, N_a is the atom density. Thus we have $\beta_{\omega_+} = \dfrac{\pi L\eta Re(\rho_{13} - \rho_{14})}{2\lambda_{\omega_+}}$, $\beta_{\omega_-} = \dfrac{-\pi L\eta Re(\rho_{23} + \rho_{24})}{2\lambda_{\omega_-}}$, $\alpha^{\pm}_{\omega_+} = \dfrac{-2\pi\eta Im(\rho_{13(4)})}{\lambda_{\omega_+}}$, and $\alpha^{\pm}_{\omega_-} = \dfrac{\pm 2\pi\eta Im(\rho_{23(4)})}{\lambda_{\omega_-}}$. Substitute the results obtained from density matrix (Eq. A.12) into Eq. A.8 and A.9, we then get the results shown in Fig 2.

[1] S. E. Harris, J. E. Field, and A. Imamoglu, Nonlinear optical processes using electromagnetically induced transparency, Phys. Rev. Lett. **64**, 1107 (1990).

[2] G. Alzetta, A. Gozzini, L. Moi, and G. Orriols, An experimental method for the observation of r.f. transitions and laser beat resonances in oriented Na vapour, Nuovo Cimento Soc. Ital. Fis. **36B**, 5 (1976).

[3] R. M. Whitley and C. R. Stroud, Jr., Double optical resonance, Phys. Rev. A **14**, 1498 (1976).

[4] R. Wynands, A. Nagel, Precision spectroscopy with coherent dark states, Appl. Phys. B **68**, 1 (1999).

[5] E. Arimondo, Coherent population trapping in laser spectroscopy, Progress in Optics **35**, 257 (1996).

[6] P. Yun, F. Tricot, C. E. Calosso, S. Micalizio, B. Francois, R. Boudot, S. Guérandel and E. de Clercq, High-performance coherent population trapping clock with polarization modulation, Phys. Rev. Applied **7,** 014018 (2017).

[7] X. Liu, E. Ivanov, V. I. Yudin, J. Kitching and E. A. Donley, Low-drift coherent population trapping Clock based on laser-cooled atoms and high-coherence excitation fields, Phys. Rev. Appl. **8**, 054001 (2017).

[8] M. Abdel Hafiz, G. Coget, M. Petersen, C. E. Calosso, S. Guérandel, E. De Clercq and R. Boudot, Symmetric autobalanced Ramsey interrogation for high-performance coherent population-trapping vapor-cell atomic clock, Appl. Phys. Lett. **112**, 244102 (2018).

[9] P. Yun, Q. Li, Q. Hao, G. Liu, E. de Clercq, S. Guérandel, X. Liu, S. Gu, Y. Gao and S. Zhang, High-performance coherent population trapping atomic clock with direct-modulation distributed Bragg reflector laser, Metrologia **58**, 054001 (2021).

[10] J. Kitching, Chip-scale atomic devices, Appl. Phys. Rev. **5,** 031302 (2018).

[11] M. Abdel Hafiz, G. Coget, E. de Clercq and R. Boudot, Doppler-free spectroscopy on the Cs D_1 line with a dual-frequency laser, Opt. Lett. **41,** 2982 (2016).

[12] D. Brazhnikov, M. Petersen, G. Coget, N. Passilly, V. Maurice, C. Gorecki and R. Boudot, Dual-frequency sub-Doppler spectroscopy: Extended theoretical model and microcell-based experiments, Phys. Rev. A **99,** 062508 (2019).

[13] A. Gusching, M. Petersen, N. Passilly, M. Abdel Hafiz, E. de Clercq and R. Boudot, Short-term stability of Cs microcell-stabilized lasers using dual-frequency sub-Doppler spectroscopy, J. Opt. Soc. Am. B **38,** 10, 3254-3260 (2021).

[14] P. D. D. Schwindt, S. Knappe, V. Shah, L. Hollberg and J. Kitching, Chip-scale atomic magnetometer, Appl. Phys. Lett. **85**, 26, 6409-6411 (2004).

[15] A. Aspect, E. Arimondo, R. Kaiser, N. Vansteenkiste, and C. Cohen- Tannoudji, Laser cooling below the one-photon recoil energy by velocity-selective coherent population trapping, Phys. Rev. Lett. **61**, 826 (1988).

[16] A. V. Taichenachev, A. M. Tumaykin, and V. I. Yudin, Quantum theory of cooling of atoms below the one-photon recoil energy by a pulsed field, JETP Lett. **65**, 779-784 (1997).

[17] M. Fleishhauer and M. D. Lukin, Dark-state polaritons in electromagnetically induced transparency, Phys. Rev. Lett. **84**, 5094 (2000).

[18] M. Bajcsy, A. S. Zibrov and M. D. Lukin, Stationary pulses of light in an atomic medium, Nature **426,** 638-641 (2003).

[19] A.M. Akulshin, S. Barreiro, and A. Lezama, Electromagnetically induced absorption and transparency due to resonant two-field excitation of quasi-degenerate levels in Rb vapor, Phys. Rev. A **57**, 2996 (1998).

[20] A.V. Taĭchenachev, A.M. Tumaikin, and V.I. Yudin, Electromagnetically induced absorption in a four-state system, Phys. Rev. A **61**, 011802(R) (1999).

[21] C. Affolderbach, S. Knappe, R. Wynands, A. V. Taĭchenachev, and V. I. Yudin, Electromagnetically induced transparency and absorption in a standing wave, Phys. Rev. A **65**, 043810 (2002).

[22] D. V. Brazhnikov, S. Ignatovizh, V. I. Vishnyakov, R. Boudot, and M. N. Skvortsov, Electromagnetically induced absorption scheme for vapor-cell atomic clock, Opt. Exp. **27**, 36034 (2019).

[23] L. Lenci, L. Marmugi, F. Renzoni, S. Gozzini, A. Lucchesini and A. Fioretti, Time-domain Ramsey-narrowed sub-kHz electromagnetically induced absorption in atomic potassium, J. Phys. B: At. Mol. Opt. Phys. **52**, 085002 (2019).

[24] J. Vanier, Atomic clocks based on coherent population trapping: A review, Appl. Phys. B **81**, 421 (2005).

[25] Y. Y. Jau, E. Miron, A. B. Post, N. N. Kuzma, and W. Happer, Push-pull optical pumping of pure superposition states, Phys. Rev. Lett. **93**, 160802 (2004).

[26] X. Liu, J. M. Merolla, S. Guérandel, C. Gorecki, E. de Clercq and R. Boudot, Coherent-population-trapping resonances in buffer-gas-filled Cs-vapor cells with push-pull optical pumping, Phys. Rev. A **87**, 013416 (2013).

[27] T. Zanon, S. Guérandel, E. De Clercq, D. Holleville, N. Dimarcq, and A. Clairon, High contrast Ramsey fringes with coherent-population-trapping pulses in a double lambda atomic system, Phys. Rev. Lett. **94**, 193002 (2005).

[28] A. V. Taichenachev, V. I. Yudin, V. L. Velichansky, and S. A. Zibrov, On the unique possibility of significantly increasing the contrast of dark resonances on the D1 line of Rb-87, JETP Letters **82**, 398-403 (2005).

[29] S. V. Kargapoltsev, J. Kitching, L. Hollberg, A. V. Taichenachev, V. L. Velichansky, and V. I. Yudin, High-contrast dark resonance in σ^+ - σ^- optical field, Laser Phys. Lett. **1**, 495-499 (2004).

[30] J. M. Danet, M. Lours, P. Yun, S. Guérandel, E. de Clercq, Frequency instability investigations on a Cs cell clock based on pulsed coherent population trapping, 2013 Joint UFFC, EFTF and PFM Symposium.

[31] X. Liu, V. I. Yudin, A. V. Taichenachev, J. Kitching and E. A. Donley, High contrast dark resonances in a cold-atom clock probed with counterpropagating circularly polarized beams, Appl. Phys. Lett. **111**, 224102 (2017).

[32] A. V. Taichenachev, V. I. Yudin, V. L. Velichansky, A. S. Zibrov, and S. A. Zibrov, Pure superposition states of atoms generated by a bichromatic elliptically polarized field, Phys. Rev. A **73**, 013812 (2006).

[33] P. Yun, J. M. Danet, D. Holleville, E. de Clercq, and S. Guérandel, Constructive polarization modulation for coherent population trapping clock, Appl. Phys. Lett. **105**, 31106 (2014).

[34] Y. Yano and S. Goka, High-Contrast Coherent Population Trapping Based on Crossed Polarizers Method, IEEE Trans. Ultrason. Ferroelec. Freq. Contr. **61**, 12, 1953-1960 (2014).

[35] M. Rosenbluh, V. Shah, S. Knappe, and J. Kitching, Differentially detected coherent population trapping resonances excited by orthogonally polarized laser fields, Opt. Express **14**, 6588 (2006).

[36] V. Gerginov, S. Knappe, V. Shah, L. Hollberg, and J. Kitching, Laser Noise Cancellation in Single-Cell CPT Clocks, IEEE Trans. Instrum. Meas. **57**, 1357 (2008).

[37] B. Tan, Y. Tian, , H. Lin, J. Chen and S. Gu, Noise suppression in coherent population trapping atomic clock by differential magneto-optic rotation detection, Opt. Lett. **40**, 16, 3703 (2015).

[38] F. Riehle, Frequency standards: basics and applications, Wiley-VCH, Weinheim, chap 3, p 77, 2004.

[39] Y. Tian, B. Z. Tan, J. Yang, Y. Zhang and S. H. Gu, Ramsey-CPT spectrum with the Faraday effect and its application to atomic clocks, Chin. Phys. B **24**, 063302 (2015).

[40] M. Abdel Hafiz and R. Boudot, A coherent population trapping Cs vapor cell atomic clock based on push-pull optical pumping, J. Appl. Phys. **118**, 124903 (2015);

[41] M. Abdel Hafiz, G. Coget, P. Yun, S. Guérandel, E. de Clercq, and R. Boudot, A high-performance Raman-Ramsey Cs vapor cell atomic clock, J. Appl. Phys. **121**, 104903 (2017).

[42] C. P. Pearman, C. S. Adams, S. G. Cox, P. F. Griffin, D. A. Smith, and I. G. Hughes, Polarization spectroscopy of a closed atomic transition: Applications to laser frequency locking, J. Phys. B **35**, 5141 (2002).

[43] B. Wang, S. Li, J. Ma, H. Wang, K. C. Peng, and M. Xiao, Controlling the polarization rotation of an optical field via asymmetry in electromagnetically induced transparency, Phys. Rev. A **73**, 051801(R) (2006).

[44] S. Li, B. Wang, X. Yang, Y. Han, H. Wang, M. Xiao, and K. C. Peng, Controlled polarization rotation of an optical field in multi-Zeeman-sublevel atoms, Phys. Rev. A **74**, 033821 (2006).